Superconducting super-organized nanoparticles of the superconductor (BEDT-TTF)2Cu(NCS)2

Dominique de Caro, Kane Jacob, Marco Revelli-Beaumont, Christophe Faulmann, Lydie Valade, Marine Tassé, Sonia Mallet-Ladeira, Shuxiang Fan, Tadashi Kawamoto, Takehiko Mori, et al.

Superconducting super-organized nanoparticles of the superconductor $(BEDT\text{-}TTF)_2Cu(NCS)_2$†

Dominique de Caro, [a,*] Kane Jacob, [a] Marco Revelli-Beaumont, [a] Christophe Faulmann, [b] Lydie Valade, [a] Marine Tassé, [a] Sonia Mallet-Ladeira, [a] Shuxiang Fan, [c] Tadashi Kawamoto, [c] Takehiko Mori [c] and Jordi Fraxedas [d]

[a] *LCC-CNRS, Université de Toulouse, CNRS, UPS, F-31077 Toulouse, France.*

[b] *CEMES-CNRS, Université de Toulouse, CNRS, UPS, F-31055 Toulouse, France.*

[c] *Department of Materials Science and Engineering, Tokyo Institute of Technology, O-okayama 2-12-1, Meguro-ku, 152-8552, Japan.*

[d] *Catalan Institute of Nanoscience and Nanotechnology (ICN2), CSIC and BIST, Campus UAB, Bellaterra, Barcelona, 08193, Spain*

ABSTRACT. The synthesis of $(BEDT\text{-}TTF)_2Cu(NCS)_2$ in the presence of poly(ethylene glycol) leads to super-organized nanoparticles of 2 to 8 nm size. Samples contain crystalline nanoparticles of the κ-$(BEDT\text{-}TTF)_2Cu(NCS)_2$ phase. The electrical conductivity at room temperature is about 0.08 $S \cdot cm^{-1}$, a typical value for nanopowders of tetrathiafulvalene-based conducting compounds. The current-voltage characteristic for an individual nanoparticle aggregate is fitted with a Shockley diode model. A saturation current of 4.1 pA and a threshold voltage of 0.45 V are extracted. N1s and S2p lines in X-ray photoelectron spectroscopy evidence a charge transfer, characteristic for tetrathiafulvalene-based conducting salts. Magnetic susceptibility studies show a superconducting transition at 9.1 K, a characteristic value for the κ-$(BEDT\text{-}TTF)_2Cu(NCS)_2$ phase. The thermoelectric power of the nanopowder is represented by the average //*c* and //*b* values for the single-crystal. Finally, resistivity for the nanopowder is nearly flat in the metallic region.

KEYWORDS. Molecular conductor, superconductor, nanoparticles.

† Electronic Supplementary Information (ESI) available: Powder X-ray diffraction diagram of BEDT_Cu_10 compared with the one calculated from crystal structure of $(BEDT\text{-}TTF)_2Cu(NCS)_2$ and list of indexed and non-indexed peaks.

1. Introduction

The family of superconductors based on the organic BEDT-TTF (bis-ethylenedithio-tetrathiafulvalene, Fig. 1) molecule is the series of molecular superconductors exhibiting the largest number of phases and the highest critical temperatures (T_c). In $(BEDT\text{-}TTF)_2X$ compounds

where X^- stands for $Cu(NCS)_2^-$, $Cu[N(CN)_2]Cl^-$ or $Cu[N(CN)_2]Br^-$, T_c are in the 8-12 K range. Black thin plate single crystals of κ-(BEDT-TTF)$_2$Cu(NCS)$_2$ are prepared by electrocrystallization, on a Pt wire, of a solution containing BEDT-TTF, Cu(NCS), KSCN and 18-crown-6 ether in 1,1,2-trichloroethane, chlorobenzene, 1,2-dichloroethane, tetrahydrofurane or ethanol [1]. The crystal structure shows that two BEDT-TTF molecules form a dimerized pair and that the dimers are arranged one another almost perpendicularly (84-87°). As a result of short intra- and inter-dimer S…S atomic contacts, the BEDT-TTF donor molecules build two-dimensional conducting sheets in the *bc*-plane. Every conducting layer is sandwiched by the insulating layers of $Cu(NCS)_2^-$ anions along the *a*-axis. This compound has also been prepared as deposits on flat conducting surfaces. For instance, thin films of (BEDT-TTF)$_2$Cu(NCS)$_2$ have been grown on indium tin oxide glass, used as the anode [2]. Films are made of plate crystals with sizes of several micrometers and exhibit a semiconducting behavior. Furthermore, nanorod arrays of κ-(BEDT-TTF)$_2$Cu(NCS)$_2$ have been produced on a platinum foil or an indium tin oxide glass [3]. The morphologies of the nanorods have been controlled by adjusting the growth current density.

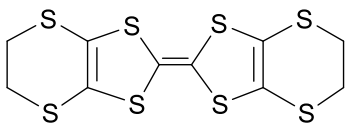

Fig. 1. Bis(ethylenedithio)tetrathiafulvalene.

We have recently reported the synthesis of nanoparticles of the kappa phase of (BEDT-TTF)$_2$Cu(NCS)$_2$. They are obtained by the reaction of BEDT-TTF and Cu(NCS)$_2$ in organic solution in the presence of, either long alkyl-chain aconitate esters [4], or *n*-dodecanoic acid [5]. These amphiphilic molecules play the role of growth controlling agent as they create steric hindrance during the particles' nucleation and the growth processes. With aconitate esters, roughly spherical nano-objects are obtained (35-120 nm in size). The largest objects are actually made of aggregated individual small particles ranging from 3 to 10 nm. With *n*-dodecanoic acid, roughly spherical nanoparticles with an average diameter of 28 nm are grown. These nanoparticles undergo a superconducting transition at 9.1 K. Besides amphiphilic molecules, neutral polymers such as poly(ethylene glycol) (Fig. 2) or polyvinylpyrrolidone have also been used to control the growth of tetrathiafulvalene-based conductors as nanoparticles [6, 7]. Poly(ethylene glycol) is an interesting polymer for stabilizing nanoparticles because it is soluble in both polar and some non-polar solvents and is quite chemically inert and non-toxic. Moreover,

it successfully stabilized TTF·TCNQ nanoparticles (TTF: tetrathiafulvalene; TCNQ: tetracyanoquinodimethane) [6]. However, in the samples, 5 to 15 % micrometre-sized platelets are observed in addition to spherical nanoparticles. In this article, we report on improved and reproducible synthesis routes producing nanoparticles of κ-$(BEDT\text{-}TTF)_2Cu(NCS)_2$ in good yield by using poly(ethyleneglycol) as growth controller, and on the superconducting transition observed for these nanoparticles at nearly the same temperature as for single crystal.

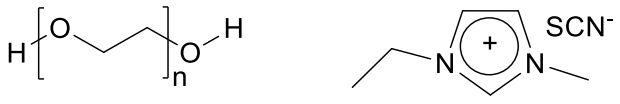

Fig. 2. Poly(ethylene glycol) (left) and 1-ethyl-3-methylimidazolium thiocyanate (right).

2. Experimental

2.1. Materials.

Solvents are degassed immediately before use. BEDT-TTF, copper(I) thiocyanate Cu(NCS), copper(II) sulfate $CuSO_4$, potassium thiocyanate KSCN, poly(ethylene glycol) 400 (n = 8-9, mean molar mass: 392 g · mol^{-1}) and 1-ethyl-3-methylimidazolium thiocyanate [EMIM][SCN] (figure 2) are commercially available and used without further purification.

2.2. Syntheses

$Cu(NCS)_2$ is prepared by adding a water solution of KSCN (1.95 g) to an aqueous acidic solution (15 % H_2SO_4) of $CuSO_4$ (1.60 g) at 0 °C. The black precipitate is filtered off, washed with water and diethylether and finally dried (yield: 65 %; elemental analysis, calculated: C 13.4 %; N 15.6 %, found: C 13.2 %; N 15.3 %).

Chemical route for the synthesis of $(BEDT\text{-}TTF)_2Cu(NCS)_2$ nanoparticles. Solution A: $Cu(NCS)_2$ (20 mg, 0.11 mmol) and PEG 400 are dissolved by stirring for 15 min in 50 mL THF at 25°C. Solution B: BEDT-TTF (80 mg, 0.21 mmol) and PEG 400 are dissolved by stirring for 15 min in 50 mL THF at 90°C. A first half of PEG 400 is added to solution A and a second half to solution B, leading to a total molar ratio of 1, 2.5, 5, 10, 15 or 20 vs. BEDT-TTF. Solution A is dropwise added to solution B at 90°C with a flow rate of 1.5 mL · min^{-1}. After stirring at 90°C for 30 min, an air-stable black solid is filtered off, washed with 3 × 10 mL hot THF, 10 mL diethyl ether, and finally dried under vacuum (yield: 65 %).

Electrochemical route for the synthesis of (BEDT-TTF)$_2$Cu(NCS)$_2$ nanoparticles. The synthesis is performed in a one-compartment electrochemical cell equipped with two platinum wire electrodes (length L = 1 cm, diameter d = 1 mm). The distance between the two electrodes is about 1 cm. The cell is filled with BEDT-TTF (60 mg, 0.16 mmol), Cu(NCS) (10 mg, 0.08 mmol), [EMIM][SCN] (34 μL, 0.24 mmol), PEG 400 (5, 10, 15, 20 molar eq. vs. BEDT-TTF) and 50 mL CH_2Cl_2. The electrolysis is conducted at 55 °C at a constant current density of ~250 $\mu A \cdot cm^{-2}$ under stirring for 1 day. The air-stable black powder of (BEDT-TTF)$_2$Cu(NCS)$_2$ is collected by filtration, washed with 5 mL portions of dichloromethane and ether, and finally dried under vacuum. Yield: 7 % for a PEG 400/BEDT-TTF molar ratio of 5, and about 55 % for 10, 15 and 20 molar ratios.

2.3. Characterization

Elemental analyses are performed by the Microanalysis Service of LCC-CNRS. Infrared spectra are taken at room temperature (in KBr matrix) on a Perkin Elmer Spectrum GX spectrophotometer. For transmission electron microscopy (TEM), the samples are sonicated in ether and placed onto a holey carbon-copper grid. Transmission electron microscopy images are taken on a JEOL Model JEM 1011 operating at 100 kV. Scanning electron microscopy (SEM) experiments are performed on a MEB-FEG JEOL JSM 7800F Prime. The sample is pasted on a carbon based, electrically conductive, double sided adhesive disc. X-ray photoelectron spectroscopy (XPS) experiments were performed using a SPECS PHOIBOS150 hemispherical analyzer with a monochromatic X-ray source (1486.6 eV) operated at 300 W in a base pressure in the low 10^{-9} mbar. The reported binding energies are referred to the Fermi level of the analyzer. The (BEDT-TTF)$_2$Cu(NCS)$_2$ powder has been dispersed on a conductive carbon tape strip (as in SEM experiments) attached to a sample holder and, after a gentle compression with a clean glass microscope slide, the excess powder is removed with nitrogen gas flow. Powder X-ray diffraction data are recorded at room temperature on a PANalytical X'Pert Pro (Theta-Theta) diffractometer with Cu $K_{\alpha1}$,$K_{\alpha2}$ radiation (λ = 1.54059, 1.54442 Å). Data collection is performed over the angular range 5° < 2θ < 90° with a step size of 0.017 °. Powder conductivity measurements are carried out on pressed pellets of pure powder materials (size: 3.14 mm^2 × 1 mm thick) without any grinding. The cylinders used to press the materials play the electrodes role. Resistance data acquisition is achieved using a Hewlett-Packard model 4263A LCR meter. Current-voltage (*I*–*V*) curves are acquired on an AFM Smarts SPM 1000 (AIST-NT) in conductivity mode using Au-coated cantilever tips (PPP-NCL Au-10 from Nanosensors. The

particles are dispersed on a gold substrate previously cleaned with acetone, water, and carefully dried. Magnetic susceptibility is measured using a MPMS-XI QUANTUM DESIGN, operating at an external magnetic field of 10 Oe on a 13.5 mg nanoparticle sample. Thermoelectric power *S* is measured using a thin film deposited from ethanol suspension of the nanopowder. The samples are attached to two copper heat blocks by carbon paste, and the heat blocks are alternately heated to generate a temperature gradient ΔT of less than 1 K [8]. The thermoelectric power was estimated from the generated voltage ΔV by $S = \Delta V/\Delta T$. By attaching gold wires with carbon paste, conductivity of the thin film was measured.

3. Results and discussion

We have reported a two-pot synthetic procedure [5] in which a THF solution of $Cu(NCS)_2$ and *n*-dodecanoic acid is added dropwise to a THF solution of BEDT-TTF and *n*-dodecanoic acid heated at 90 °C. Nanocrystalline κ-$(BEDT\text{-}TTF)_2Cu(NCS)_2$ precipitates as a black solid. In the present paper, we have applied the same synthetic route by replacing *n*-dodecanoic acid by PEG 400. Whatever the PEG 400/BEDT-TTF molar ratio (1, 2.5, 5, 10, 15, 20), the infrared spectrum exhibits two CN vibration modes at ~2067 and ~2109 cm^{-1} which are the adequate peaks found in the infrared spectrum of microcrystalline κ-$(BEDT\text{-}TTF)_2Cu(NCS)_2$. However, electron micrographs of these six samples exhibit a majority of micrometre-sized platelets and a few amount of nanoparticles (10 to 70 nm in size). This chemical method does not allow the selective preparation of nanoparticles and has not been investigated further.

We have previously described the electrochemical synthesis of κ-$(BEDT\text{-}TTF)_2Cu(NCS)_2$ as very small nanoparticles [9]. This electrochemical route was performed in a two-compartment electrochemical cell containing BEDT-TTF, Cu(NCS) and the ionic liquid [EMIM][SCN] ($EMIM^+$: 1-ethyl-3-methyl imidazolium, figure 2), acting as supporting electrolyte, provider of an additional SCN^- ligand, and finally as a growth controller. The black solid grown on the anode exhibited well dispersed nanoparticles (mean size: 10 nm). However, this electrochemical route led to relatively low yields (about 20 %) and did not show the required reproducibility.

In the present paper, we have studied the combined addition of [EMIM][SCN] and PEG 400 on the electrochemical growth of $(BEDT\text{-}TTF)_2Cu(NCS)_2$. In that respect, in a one-compartment electrochemical cell, we have performed the oxidation of BEDT-TTF in a dichloromethane solution of Cu(NCS), [EMIM][SCN] (3 molar eq. vs. Cu(NCS)) and PEG 400 (5 to 20 molar eq. vs. BEDT-TTF) at 55 °C at a constant current density of ~250 $\mu A \cdot cm^{-2}$.

For a PEG 400/BEDT-TTF molar ratio of 5, the yield is about 7 %. For PEG 400/BEDT-TTF molar ratios of 10, 15 and 20, yields are close to 55 %. Only these last three samples have been further investigated. Their infrared spectra show the two CN vibration modes at 2067 and 2110 cm^{-1} assigned to κ-$(BEDT\text{-}TTF)_2Cu(NCS)_2$.

For molar ratios of 15 and 20, electron micrographs show a majority of nanoparticles (10 to 70 nm in size) in addition to a few amount of micrometre-sized platelets. For a PEG 400/BEDT-TTF molar ratio of 10 (sample further abbreviated as BEDT_Cu_10), electron micrographs evidence the exclusive presence of nanoparticles (Fig. 3). Several possible reasons can explain the control of the growth of $(BEDT\text{-}TTF)_2Cu(NCS)_2$ as nanoparticles in the presence of both [EMIM][SCN] and PEG 400. We first assume that π–π interactions can occur between the heterocycle of $EMIM^+$ and those of BEDT-TTF. Secondly, PEG 400 can adsorb onto the platinum electrode surface. Therefore, the nucleation process of $(BEDT\text{-}TTF)_2Cu(NCS)_2$ is more closely controlled at the electrode-solution interface, and the growth process is quickly blocked due to the sterically hindered PEG 400, leading to nanoparticles. As mentioned above, BEDT_Cu_10 is only made of nanoparticles (no micron-sized platelets are observed). Furthermore, it interestingly exhibits nanoparticles organized in domains (Fig. 3). Their individual sizes are in the 2-8 nm range. They are smaller than those prepared with the only [EMIM][SCN] as growth controller (90 % of the particles with sizes in the 8-15 nm range) [9]. This shows the effective combination of [EMIM][SCN] and PEG 400 (10 molar eq. vs. BEDT-TTF) in the growth control and organization of $(BEDT\text{-}TTF)_2Cu(NCS)_2$ particles.

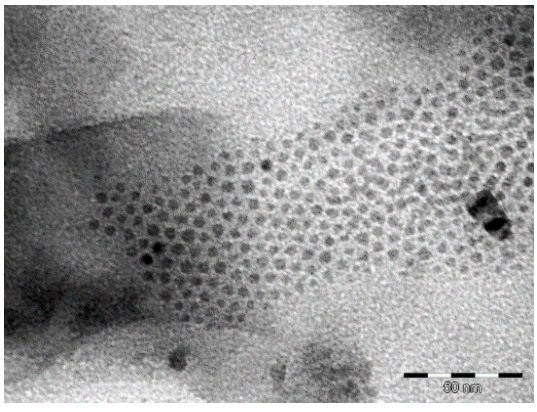

Fig. 3. TEM image for BEDT_Cu_10 (bar = 50 nm).

Scanning electron micrographs confirm the presence of roughly spherical nanoparticles (Fig. 4). Layers of hexagonal superstructures recall the organisation observed by TEM on Fig. 3 for a single layer of nanoparticles: these layers organise along stacks which end with a cauliflower-shaped structure.

The powder X-Ray diffraction diagram (ESI†) is in agreement with that of the κ-(BEDT-TTF)$_2$Cu(NCS)$_2$ phase, alike the one previously reported [9, 10].

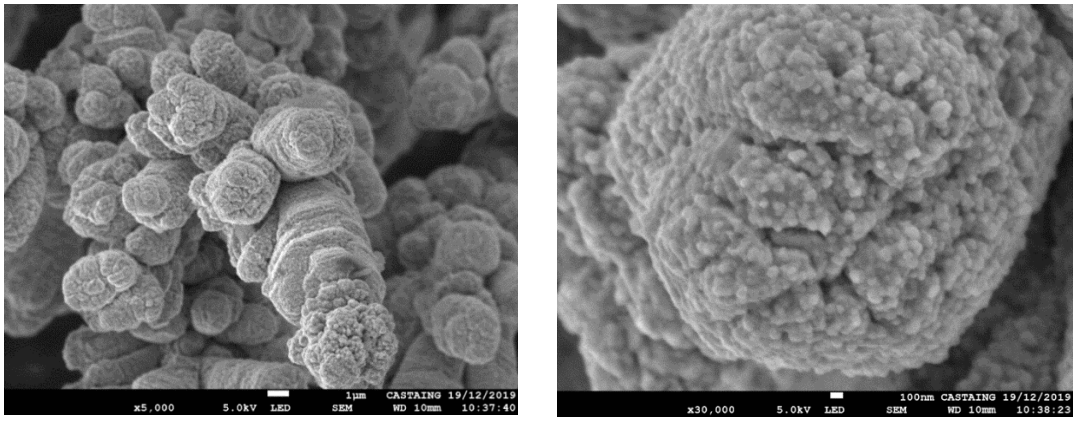

Fig. 4. SEM images for BEDT_Cu_10 (left: bar = 1 μm; right: bar = 100 nm).

Infrared spectrum for BEDT_Cu_10 is shown in Fig. 5. The ν_{C-S} stretching mode is observed at 875 (m, ν_{49} b_{2u}) cm^{-1}, a similar value to that reported for a polycrystalline powder of κ-(BEDT-TTF)$_2$Cu(NCS)$_2$ [11], *i.e.*, 880 (m) cm^{-1}. The $\nu_{C=C}$ stretching vibrations are located at 1445 (m, ν_{27} b_{1u}), 1408 (m, ν_{27} b_{1u}) and 1316 (s, ν_3 a_g) cm^{-1}. Their positions are very close to those reported for polycrystalline samples [11]: 1445 (w), 1408 (w) and 1320 (vs) cm^{-1}. The two bands at 1445 and 1408 cm^{-1} are assigned to the same ν_{27} b_{1u} vibration mode. The authors of ref. 11 assume that this mode is coupled with the intramolecular charge transfer. This fact supports the occurrence of electron-molecular vibration (e-mv) coupling with ν_{27} b_{1u} mode. As we also observe these two infrared bands in BEDT_Cu_10, e-mv couplings are also present in the nanocrystalline powder, thus confirming the conducting character of the sample. BEDT_Cu_10 exhibits a room-temperature conductivity of about 0.08 S · cm^{-1}. This value is much lower than that reported for a κ-(BEDT-TTF)$_2$Cu(NCS)$_2$ microcrystalline powder (about 10 S · cm^{-1}) [12]. Nanoparticles could be covered by ionic liquid and/or polymer, presumably as a very thin shell at the particle surface. This results in an increase of interparticle resistances in comparison with microcrystalline powders, leading to lower electrical conductivities.

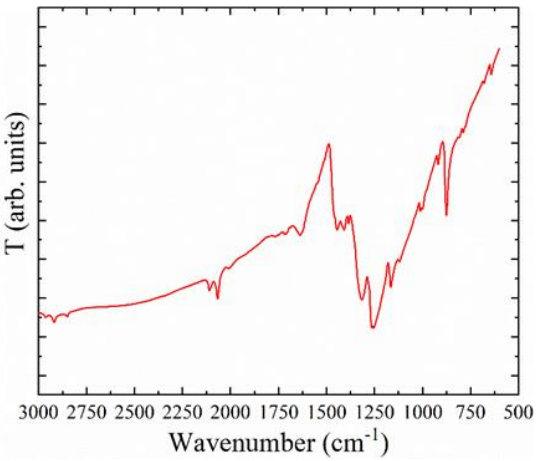

Fig. 5. Infrared spectrum for BEDT_Cu_10.

Fig. 6 shows high resolution experimental XPS spectra (black dots) of the N1s (Fig. 6(a)) and S2p lines (Fig. 6(b)), respectively, with the corresponding least-squares fits using the CasaXPS software [13], after a Shirley-type background subtraction (continuous grey line) using a combination of Gaussian (90 %) and Lorentzian (10 %) functions under the constraint of identical full width at half maximum (FWHM) for all components. The envelope from the fits, represented by orange lines, closely follows the experimental data. Fig. 6(c) shows the spectrum corresponding to the Cu2p core level region. The N1s core level region exhibits two main features at 398.3 (red line) and 401.7 eV (olive line), respectively, and a shoulder at 399.7 eV (blue line). Both 398.3 and 401.7 eV lines are ascribed to the contributions for $Cu(NCS)_2^-$ (and perhaps also from residual SCN^- anions) [14] and $EMIM^+$ [15], respectively. We assign the 399.7 eV shoulder to neutral Cu(NCS) species, in analogy to similar contributions observed in TCNQ salts [16, 17]. We thus observe, apart from the contribution from $Cu(NCS)_2^-$ anion, the presence of 1-ethyl-3-methylimidazolium, which was not completely eliminated after the purification of the synthesized powder. Fig. 6(b) shows a complex line shape for the S2p core level. Here, the least-squares fit has been performed with a fixed spin-orbit splitting of 1.18 eV and a $S2p_{1/2}$ to $S2p_{3/2}$ branching ratio of 0.5 for all components. The main feature (blue line at 163.6 eV) corresponds to neutral BEDT-TTF species while the contribution from $BEDT\text{-}TTF^+$ is located at 164.6 eV (red line). The observation of both species is characteristic from charge transfer salts, as previously discussed in the literature [17, 18]. According to Itti et al. [14], the contribution from $Cu(NCS)_2^-$ should have a binding energy of about 165.5 eV, which corresponds to the green line in the Fig. 6(b). In addition, we observe a contribution from the $CuSO_4$ used in the preparation of the starting $Cu(NCS)_2$ complex, represented by the (wine) line with 168.3 eV binding energy. Finally, two weak features at lower energies, namely at 161.8 eV (olive line) and 162.4 eV (magenta line), are also observed. Such energies are too low for the

characteristic C–S bonds but are in the range of metal-sulfur bonds [19], so that it may tentatively be assigned to Cu–S that may have formed during the electrochemical reaction. From Fig. 6(c), we observe that the main contribution from copper is the Cu(I) configuration, with traces of Cu(II) most probably from residual $CuSO_4$ used in the preparation of the starting $Cu(NCS)_2$ complex.

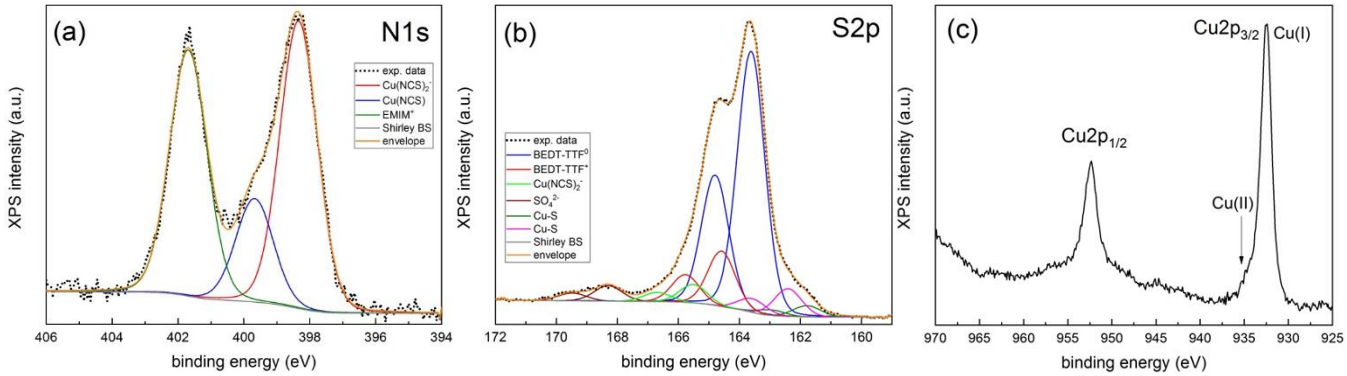

Fig. 6 High resolution XPS spectra for BEDT_Cu_10 corresponding to (a) N1s, (b) S2p and (c) Cu2p core levels of the as-received sample. Details of the least-squares fits are given in the main text.

Fig. 7(a) shows the *I–V* curve of an individual nanoparticle aggregate obtained from conductive atomic force microscopy. The non-linearity of the *I-V* curve might be attributed to the non-Ohmic character of the contact due to an imperfect interface between the tip and the nanoparticle aggregate. In the linear part of the curve, the observed energy gap is about 0.95 eV. A least-squares fit of the region corresponding to positive bias voltages (from 0.00 to 2.00 V) is shown on Fig. 7(b). The fit is obtained using the Shockley diode equation:

$$I = I_0 \left[e^{\frac{V}{V_0}} - 1 \right]$$

where I_0 represents the saturation current and V_0 the threshold voltage (energy barrier). From the fit, we obtain I_0 = 4.1 ± 0.1 pA and V_0 = 0.450 ± 0.004 V (coefficient of determination: R^2 = 0.998). The activation energy barrier extracted from the fit, *i.e*. 0.450 eV, is in relatively good agreement with half of the energy gap (0.95/2 = 0.475 eV).

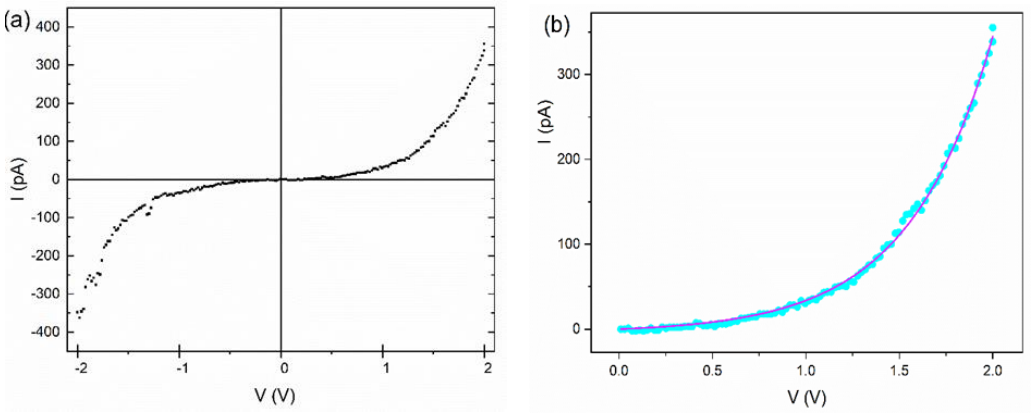

Fig. 7. *I-V* curve for an individual nanoparticle aggregate (a) and least-square fit of the positive bias voltage (b).

Fig. 8 shows the d.c. volume susceptibility (χ_{vol}) of BEDT_Cu_10 as a function of temperature. The volume magnetic susceptibility is measured at 10 Oe in zero-field cooling (ZFC) and field cooling (FC) mode. ZFC represents the effect of diamagnetic shielding whereas FC represents the effect of magnetic field expulsion (Meissner effect). The magnetization starts to decrease at 9.1 K. This temperature corresponds to the superconducting transition temperature (T_c) of BEDT_Cu_10 nanoparticles. The critical temperature value measured on nanoparticles is very close to that for bulk κ-(BEDT-TTF)$_2$Cu(NCS)$_2$ measured in the ZFC/FC mode at 100 Oe (9.4 K) [20]. A similar effect has been observed for colloidal Pb nanoparticles, where T_c = 6.9 K for diameters between 16 and 20 nm while for bulk lead the critical temperature is 7.2 K [21]. The Meissner (FC) to shielding susceptibility (ZFC) ratio gives a lower bound to the superconducting volume fraction. From the ratio $\chi_{vol\ (FC)}$ / $\chi_{vol\ (ZFC)}$ measured at 10 Oe and 2 K, we estimate a superconducting volume fraction of about 30 % for BEDT_Cu_10. It should be noted that it is a rough estimation since the anisotropy and demagnetization factors may modify this value. By taking this remark into account, the FC-ZFC ratio obtained for BEDT_Cu_10 is in agreement with those of previously isolated 28 nm diameter nanoparticles [5] and bulk [22] κ-(BEDT-TTF)$_2$Cu(NCS)$_2$ (about 40 %). The dispersed nanoparticles observed by TEM (figure 3) are actually organized as nanoparticle aggregates (sizes in the 40-100 nm range, as evidenced by SEM, Fig. 4). This super-structure organisation do not prevent superconductivity to develop and occur at a critical temperature similar to that for bulk κ-(BEDT-TTF)$_2$Cu(NCS)$_2$, in line with previous results observed for nanoparticles of Bechgaard salts [23]. These results indicate that the coherence length is shorter than 40 nm, in agreement with data for the bulk (7.5 nm for the in-plane coherence length and 0.5 nm for the out-of-plane coherence length) [24].

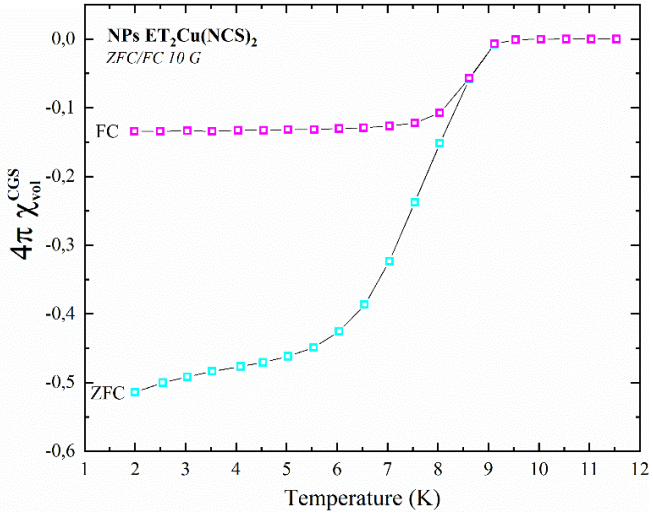

Fig. 8. Temperature dependence of the d.c. volume susceptibility in the zero-field cooling (ZFC) and field cooling (FC) mode for BEDT_Cu_10.

As shown in Fig. 9, the thermoelectric power *S* of the nanopowder is close to zero. This is contrasting to the thermoelectric power for the single crystal [25], which is comparatively large, reflecting the strong correlation [26]. The thermoelectric power of the single crystal is, however, positive for //*c*, while negative for //*b* owing to the Fermi surface [26]. The nanopowder *S* is approximated by the average. This is reasonable if the nanopowder *S* is represented by the weighted average

$$S = \frac{\sigma_c S_c + \sigma_b S_b}{\sigma_c + \sigma_b}$$

and approximately $\sigma_c = \sigma_b$.

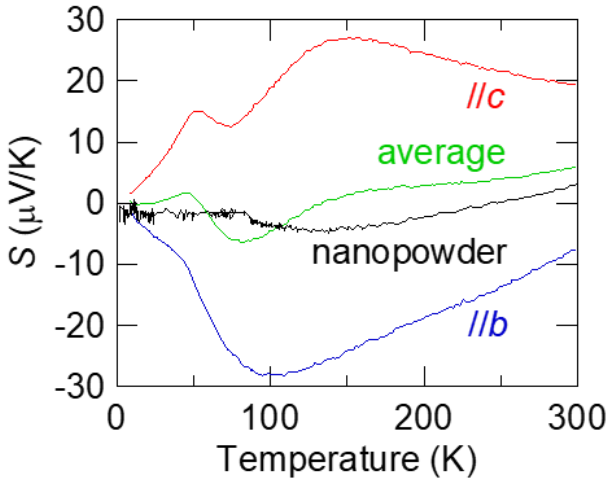

Fig. 9. Thermoelectric power *S* for BEDT_Cu_10 nanopowder together with the single crystal results.[25]

Resistivity of the nanoparticle film is shown in Figure 10. The single crystal resistivity increases down to 100 K due to the strong correlation, but turns to metallic below 100 K [27]. In the nanoparticles, the resistivity is nearly flat in the metallic region, but the slope changes around 100 K.

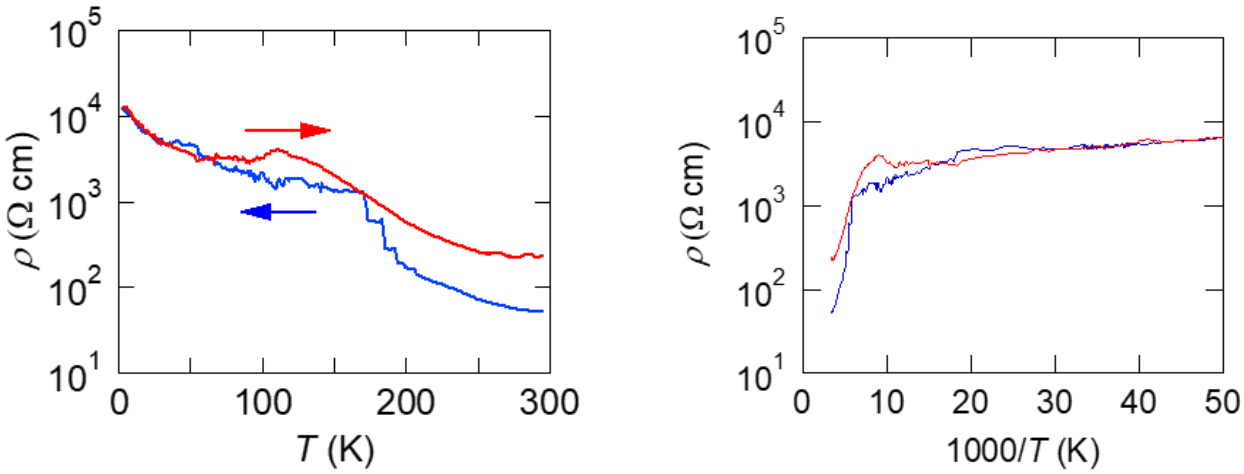

Fig. 10. Resistivity for BEDT_Cu_10, measured in the cooling and heating runs (vs. *T*, left; vs. *1/T*, right).

4. Conclusion

In this paper, we reported on the electrosynthesis of super-organized nanoparticles of the molecular superconductor κ-(BEDT-TTF)$_2$Cu(NCS)$_2$. The growth controller was a combination of an imidazolium-based ionic liquid, *i.e.* [EMIM][SCN], and poly(ethylene glycol). According to transmission electron microscopy, their sizes were in the 2-8 nm range and XPS evidences the presence of charge transfer. This low size was remarkable for tetrathiafulvalene-based materials which usually tended to grow as elongated objects and does not affect the structure of this molecular conductor, as reflected by the X-ray diffraction pattern. Magnetic measurements in zero-field cooling and field cooling mode confirmed the observation of a superconducting transition at $T_c \sim 9.1$ K for nanoparticles. Finally, the resistivity for nanoparticle powders is nearly flat in the metallic region. Despite a low electrical conductivity of about 10^{-1} S · cm^{-1}, this material might have a potential interest in organic thermoelectric devices since their morphology should favor a lower thermal conductivity thanks to the nanoscale size of the particles, and then this should increase the thermoelectric figure of merit, ZT. Works are currently in progress to determine ZT.

Author Contributions

D.d.C., L.V. and C.F. initiated this work. They also conceived and designed the syntheses and, finally, they wrote the paper. K.J. performed nanoparticle syntheses and characterization of the samples by electron microscopy (TEM and SEM). M.R-B. performed infrared analysis and magnetic susceptibility measurements. M.T. recorded current-voltage curves. S.M-L. performed and interpreted powder X-ray diffraction. S.F., T.K. and T.M. performed resistivity measurements and investigated the thermoelectric power on nanoparticles, both in a large temperature range. J.F. investigated X-ray photoelectron spectroscopy on nanoparticle powders.

Conflicts of interest

There are no conflicts to declare.

Acknowledgements

This work has been supported by the Centre National de la Recherche Scientifique (CNRS). M. R. B. thanks the Ministère de l'Enseignement Supérieur et de la Recherche for a doctoral grant. This research was supported by the Spanish Ministry of Economy and Competitiveness (MINECO) under Contract No. PGC2018-095032-B-100. The ICN2 is funded by the CERCA program/Generalitat de Catalunya. The ICN2 is supported by the Severo Ochoa program of MINECO (Grant SEV-2017-0706). This work was partly supported by the JSPS KAKENHI Grant Number 18H02044, and the Takahashi Industrial and Economic Research Foundation (08-003-022).

References

[1] G. Saito, Physica C, 162-164 (1989) 577-582. https://doi.org/10.1016/0921-4534(89)91162-3.

[2] H. Awano, K. Kawase, M. Asai, H. Ohigashi, S. Ohshima, K. Akiyama and M. Kato, Japanese Journal of Applied Physics, 31 (1992) 1899-1900. https://iopscience.iop.org/article/10.1143/JJAP.31.1899.

[3] C. S. Huang, Y. Zhang, H. B. Liu, S. Cui, C. R. Wang, L. Jiang, D. P. Yu, Y. L. Li and D. B. Zhu, Journal of Physical Chemistry C, 111 (2007) 3544-3547. https://doi.org/10.1021/jp067449k.

[4] B. Cormary, C. Faulmann, D. de Caro, L. Valade, P. de Caro, B. Ballesteros and J. Fraxedas, Comptes Rendus Chimie, 21 (2018) 809-813. https://doi.org/10.1016/j.crci.2018.07.006.

[5] M. Revelli-Beaumont, C. Faulmann, D. de Caro, M. Cazayous, Y. Gallais, A. Sacuto, C. Pasquier, P. Auban Senzier, M. Monteverde, K. Jacob and L. Valade, Synthetic Metals, 261 (2020) 116310. https://doi.org/10.1016/j.synthmet.2020.116310.

[6] D. de Caro, L. Valade, C. Faulmann, K. Jacob, D. Van Dorsselaer, I. Chtioui, L. Salmon, A. Sabbar, S. El Hajjaji, E. Perez, S. Franceschi and J. Fraxedas, New Journal of Chemistry, 37 (2013) 3331-3336. http://dx.doi.org/10.1039/C3NJ00555K.

[7] T. Kadoya, D. de Caro, K. Jacob, C. Faulmann, L. Valade and T. Mori, Journal of Materials Chemistry, 21 (2011) 18421-18424. http://dx.doi.org/10.1039/C1JM12783G.

[8] R. Sato, Y. Kiyota, T. Kadoya, T. Kawamoto and T. Mori, RSC Advances, 6 (2016) 41040-41044. https://doi.org/10.1039/C6RA04455G.

[9] D. de Caro, C. Faulmann, L. Valade, K. Jacob and B. Cormary, French-Ukrainian Journal of Chemistry, 4 (2016) 65-75. http://dx.doi.org/10.17721/fujcV4I1P65-75.

[10] Crystallographic data: Monoclinic, Space group $P2_1$; refined cell for BEDT_Cu_10: a = 16.255(3), b = 8.457(1), c = 13.142(3) Å ; β = 110.297(3) ; V = 1694.5 $Å^3$ to be compared to a = 16.256(3), b = 8.4564(13), c = 13.143(3) Å ; β = 110.276(14)°; V = 1694.776 $Å^3$. .

[11] R. Swietlik, C. Garrigou-Lagrange, C. Sourisseau, G. Pages and P. Delhaes, Journal of Materials Chemistry, 2 (1992) 857-864. https://doi.org/10.1039/JM9920200857.

[12] T. Mori, Electronic properties of organic conductors, 1st ed., Springer, 2016.

[13] J. Walton, P. Wincott, N. Fairley and A. Carrick, Peak Fitting with CasaXPS Accolyte Science, Knutsford, UK, 2010.

[14] R. Itti, H. Mori, K. Ikeda, I. Hirabayashi, N. Koshizuka and S. Tanaka, Physica C, 185 (1991) 2673-2674. https://doi.org/10.1016/0921-4534(91)91458-G.

[15] O. Höfft, S. Bahr, M. Himmerlich, S. Krischok, J. A. Schaefer and V. Kempter, Langmuir, 22 (2006) 7120-7123. https://doi.org/10.1021/la060943v.

[16] C. Rojas, J. Caro, M. Grioni and J. Fraxedas, Surface Science, 482-5 (2001) 546-551. https://doi.org/10.1016/S0039-6028(01)00715-4.

[17] M. Sing, U. Schwingenschlögl, R. Claessen, M. Dressel and C. S. Jacobsen, Physical Review B, 67 (2003) 125402. https://doi.org/10.1103/PhysRevB.67.125402.

[18] J. Fraxedas, S. García-Gil, S. Monturet, N. Lorente, I. Fernández-Torrente, K. J. Franke, J. I. Pascual, A. Vollmer, R. P. Blum, N. Koch and P. Ordejón, Journal of Physical Chemistry C 115 (2011) 18640-18648. https://doi-org.inc.bib.cnrs.fr/10.1021/jp2050838.

[19] I. Malfant, K. Rivasseau, J. Fraxedas, C. Faulmann, D. De Caro, L. Valade, L. Kaboub, J. M. Fabre and F. Senocq, Journal of the American Chemical Society, 128 (2006) 5612-5613. https://doi-org.inc.bib.cnrs.fr/10.1021/ja060690s.

[20] M. Tokumoto, H. Anzai, K. Takahashi, K. Murata, N. Kinoshita and T. Ishiguro, Synthetic Metals, 27 (1988) A305-A310. https://doi.org/10.1016/0379-6779(88)90416-X.

[21] P. Zolotavin and P. Guyot-Sionnest, ACS Nano, 4 (2010) 5599-5608. 10.1021/nn102009g.

[22] H. Veith, C.-P. Heidmann, H. Müller, H. P. Fritz, K. Andres and H. Fuchs, Synthetic Metals, 27 A (1988) 361-365. https://doi.org/10.1016/0379-6779(88)90424-9.

[23] L. E. Winter, E. Steven, J. S. Brooks, S. Benjamin, J.-H. Park, D. de Caro, C. Faulmann, L. Valade, K. Jacob, I. Chtioui, B. Ballesteros and J. Fraxedas, Physical Review B, 91 (2015) 035437. https://doi.org/10.1103/PhysRevB.91.035437.

[24] S. Friemel, C. Pasquier, Y. Loirat and D. Jerome, Physica C, 259 (1996) 181-186. https://doi.org/10.1016/0921-4534(95)00809-8.

[25] H. Urayama, H. Yamochi, G. Saito, T. Sugano, M. Kinoshita, T. Inabe, T. Mori, Y. Maruyama and H. Inokuchi, Chemistry Letters, (1988) 1057-1060. https://doi.org/10.1246/cl.1988.1057.

[26] T. Mori and H. Inokuchi, Journal of the Physical Society of Japan, 57 (1988) 3674-3677. https://doi.org/10.1143/JPSJ.57.3674.

[27] H. Urayama, H. Yamochi, G. Saito, K. Nozawa, T. Sugano, M. Kinoshita, S. Sato, K. Oshima, A. Kawamoto and J. Tanaka, Chemistry Letters, 17 (1988) 55-58. https://doi.org/10.1246/cl.1988.55.

Superconducting super-organized nanoparticles of the superconductor $(BEDT\text{-}TTF)_2Cu(NCS)_2$

ESI content

- Powder X-ray diffraction diagram of BEDT_Cu_10 compared with the one calculated from crystal structure of $(BEDT\text{-}TTF)_2Cu(NCS)_2$
- List of indexed and non-indexed peaks.

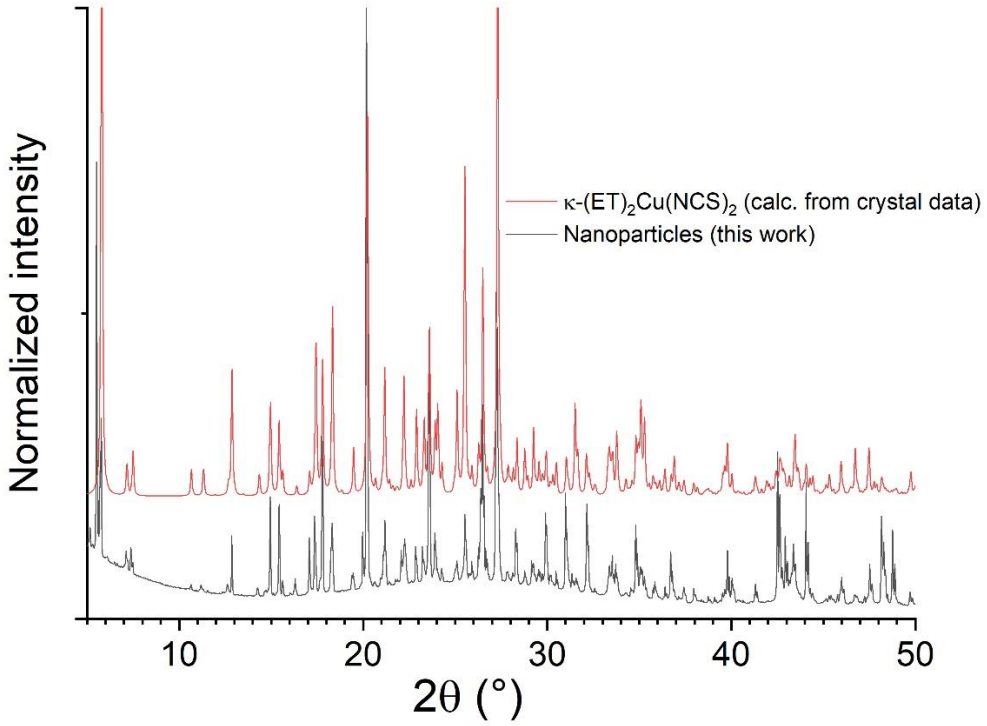

Powder X-ray diffraction diagram of BEDT_Cu_10 compared with the one calculated form crystal structure of $(BEDT\text{-}TTF)_2Cu(NCS)_2$

Relevant parameters of BEDT_Cu_10

Bibliographic data:	
Audit creation date:	1989-01-20
Audit creation method:	CSD-ConQuest-V1
Author name:	K.D.Carlson, U.Geiser, A.M.Kini, H.H.Wang, L.K.Montgomery, W.K.Kwok, M.A.Beno, J.M.Williams, C.S.Cariss, G.W.Crabtree
Chemical name systematic:	bis(bis(Ethylenedithio)tetrathiafulvalene) di-isothiocyanato-copper
Formula sum:	$C_{22}H_{16}Cu_1N_2S_{18}$
Journal name:	Inorg.Chem.
Journal volume:	27
Page first:	965
Structure and profile data:	
Formula sum:	$Cu_{2.00}S_{36.00}N_{4.00}C_{44.00}$
Formula mass/ g/mol:	1865.7630
Density (calculated)/ g/cm^3	1.8281
F(000):	926.0000
Mass Absorption Coefficient/ cm^2/g:	60.4901
Volume fraction/ %:	100.0000
Weight fraction/ %:	100.000000
Space group (No.):	P 1 21 1 (4)
Lattice parameters:	
a/ Å:	16.255(3)
b/ Å:	8.457(1)
c/ Å:	13.142(3)
alpha/ °:	90
beta/ °:	110.297(3)
gamma/ °:	90
V/ 10^6 pm^3	1694.50000

Non-indexed peaks

No.	2Th. (o) [°]	d-sp. (o) [Å]	Rel. Int. [%]
1	5.1628	17.103160	4.36
2	5.5102	16.025440	67.50
3	5.6083	15.745310	9.25
4	7.3804	11.968240	5.28
5	19.9724	4.442046	10.33
6	26.5557	3.353881	15.26

Indexed peaks

No.	h	k	l	2Th. (c) [°]	2Th. (o) [°]	2Th. (d) [°]	d-sp. (c) [Å]	d-sp. (o)
1	1	0	0	5.7922	5.7623	0.0300	15.245800	15.325000
2	0	0	1	7.1660	7.1440	0.0219	12.325950	12.363710
3	1	0	-1	7.4914	7.4780	0.0134	11.791270	11.812310
4	1	0	1	10.6724	10.6448	0.0275	8.282834	8.304196
5	2	0	-1	11.3251	11.1930	0.1321	7.806897	7.898732
6	0	1	1	12.6836	12.6176	0.0659	6.973598	7.009898
7	1	1	-1	12.8713	12.8673	0.0040	6.872332	6.874458
8	0	0	2	14.3601	14.2664	0.0938	6.162977	6.203271
9	1	1	1	14.9590	14.9488	0.0102	5.917564	5.921581
10	2	1	-1	15.4341	15.4351	-0.0011	5.736479	5.736083
11	2	0	1	15.6337	15.6250	0.0087	5.663672	5.666799
12	3	0	-1	16.3862	16.3036	0.0826	5.405236	5.432424
13	1	1	-2	17.0945	17.0704	0.0241	5.182831	5.190095
14	3	0	0	17.4365	17.3579	0.0786	5.081934	5.104771
15	0	1	2	17.7934	17.7675	0.0260	4.980797	4.988015
16	2	1	-2	18.3290	18.3089	0.0201	4.836457	4.841716
17	3	1	-1	19.4744	19.4249	0.0495	4.554492	4.565980
18	1	1	2	20.2326	20.1784	0.0542	4.385503	4.397159
19	3	1	-2	21.1719	21.1867	-0.0148	4.193003	4.190116
20	0	2	1	22.2072	22.0597	0.1475	3.999811	4.026228
21	1	2	-1	22.3168	22.2631	0.0537	3.980421	3.989901
22	1	1	-3	22.9056	22.8539	0.0517	3.879411	3.888078
23	2	1	-3	23.2235	23.2175	0.0060	3.827029	3.827996
24	3	1	1	23.5799	23.5778	0.0020	3.769989	3.770312
25	2	1	2	23.9052	23.8928	0.0124	3.719414	3.721313
26	1	0	3	24.2932	24.2813	0.0119	3.660871	3.662644
27	4	1	-2	25.1061	25.0883	0.0177	3.544160	3.546625
28	0	2	2	25.5260	25.5298	-0.0038	3.486799	3.486286
29	2	2	-2	25.9086	25.9001	0.0085	3.436166	3.437273
30	2	2	1	26.2804	26.2533	0.0271	3.388396	3.391828
31	3	0	2	26.2959	26.3959	-0.1000	3.386436	3.373831
32	1	1	3	26.5095	26.4980	0.0116	3.359625	3.361065
33	3	2	-1	26.7453	26.6547	0.0906	3.330540	3.341653

34	2	0	-4	27.1706	27.2275	-0.0569	3.279361	3.272642
35	3	1	2	28.3665	28.2786	0.0878	3.143775	3.153341
36	4	1	1	28.7909	28.7974	-0.0065	3.098384	3.097704
37	2	1	-4	29.1839	29.1456	0.0384	3.057549	3.061486
38	3	2	1	29.9193	29.8965	0.0228	2.984052	2.986274
39	2	2	2	30.1809	30.1890	-0.0081	2.958782	2.958005
40	4	2	-1	30.4968	30.4730	0.0237	2.928848	2.931075
41	3	2	-3	31.0392	30.9865	0.0527	2.878890	2.883664
42	4	2	-2	31.1574	31.3351	-0.1777	2.868239	2.852376
43	4	0	2	31.5683	31.5559	0.0124	2.831836	2.832922
44	4	1	-4	32.1303	32.1442	-0.0140	2.783575	2.782398
45	5	0	-4	33.3835	33.3772	0.0063	2.681890	2.682383
46	1	3	1	33.5526	33.5318	0.0208	2.668756	2.670364
47	2	3	-1	33.7773	33.7209	0.0563	2.651520	2.655820
48	1	2	-4	34.8073	34.8034	0.0039	2.575377	2.575657
49	5	2	-2	35.0590	35.0529	0.0060	2.557462	2.557889
50	6	1	-1	35.1067	35.1561	-0.0494	2.554094	2.550619
51	6	0	0	35.2940	35.2855	0.0085	2.540967	2.541560
52	2	1	-5	35.7551	35.7575	-0.0025	2.509252	2.509085
53	4	0	-5	35.8397	35.8402	-0.0005	2.503519	2.503485
54	1	1	-5	36.3962	36.3916	0.0046	2.466509	2.466812
55	5	2	-3	36.7349	36.7072	0.0277	2.444543	2.446324
56	3	3	-2	36.8920	36.8869	0.0050	2.434492	2.434813
57	4	1	-5	37.4328	37.4329	-0.0001	2.400550	2.400545
58	1	3	-3	37.9624	37.9659	-0.0036	2.368274	2.368059
59	7	0	-2	38.7470	38.7478	-0.0007	2.322101	2.322059
60	5	2	1	39.0791	39.0760	0.0031	2.303131	2.303307
61	6	2	-2	39.5417	39.5291	0.0126	2.277246	2.277942
62	5	1	-5	39.6442	39.6453	-0.0011	2.271595	2.271533
63	6	2	-1	39.7978	39.7865	0.0113	2.263177	2.263795
64	6	1	1	40.0478	40.0440	0.0037	2.249627	2.249829
65	4	3	-3	41.3002	41.3037	-0.0035	2.184252	2.184075
66	5	3	-1	42.5124	42.5084	0.0041	2.124733	2.124926
67	6	1	-5	42.6280	42.6328	-0.0047	2.119238	2.119014
68	2	1	-6	42.7466	42.7674	-0.0208	2.113637	2.112655

69	3	3	-4	42.9185	42.9352	-0.0167	2.105568	2.104787
70	1	4	0	43.1614	43.1480	0.0133	2.094279	2.094895
71	4	2	3	43.1914	43.2851	-0.0936	2.092891	2.088580
72	0	4	1	43.3875	43.3738	0.0137	2.083887	2.084512
73	5	3	-3	44.0730	44.0603	0.0127	2.053052	2.053615
74	6	1	2	44.2922	44.2823	0.0098	2.043400	2.043831
75	7	1	1	45.9924	45.9955	-0.0032	1.971739	1.971611
76	5	3	-4	46.7107	46.7097	0.0010	1.943079	1.943118
77	3	3	-5	47.5328	47.5243	0.0086	1.911370	1.911694
78	6	0	3	48.1612	48.1633	-0.0022	1.887891	1.887810
79	0	4	3	48.3762	48.3579	0.0183	1.879999	1.880667
80	5	0	4	48.7184	48.7636	-0.0452	1.867591	1.865966
81	3	1	-7	49.7051	49.7093	-0.0042	1.832805	1.832660
82	7	1	2	50.1595	50.1684	-0.0090	1.817261	1.816957
83	4	4	1	51.1333	51.1257	0.0076	1.784914	1.785162
84	1	2	6	51.6075	51.5936	0.0139	1.769621	1.770067
85	5	4	-3	52.9642	52.9837	-0.0194	1.727444	1.726856
86	1	3	-6	53.7961	53.7945	0.0016	1.702679	1.702726
87	4	4	2	54.0872	54.0900	-0.0027	1.694198	1.694120
88	2	2	6	54.5888	54.5902	-0.0015	1.679813	1.679771
89	7	1	3	55.1849	55.1886	-0.0037	1.663068	1.662967
90	4	2	5	55.3163	55.3315	-0.0152	1.659429	1.659010
91	7	3	1	55.8042	55.8184	-0.0142	1.646070	1.645686
92	9	2	-1	56.5164	56.5263	-0.0099	1.627006	1.626744
93	3	5	-1	57.0031	57.0288	-0.0258	1.614266	1.613598
94	3	5	-2	57.7032	57.6818	0.0214	1.596332	1.596874
95	5	4	-5	58.5906	58.6012	-0.0105	1.574252	1.573994
96	7	4	-2	59.0391	59.0351	0.0040	1.563359	1.563455
97	7	3	-6	59.7805	59.7786	0.0019	1.545728	1.545773
98	4	5	-3	60.9353	60.9373	-0.0020	1.519172	1.519128
99	4	4	-6	61.5236	61.5296	-0.0060	1.506050	1.505917
100	6	4	2	62.1657	62.1457	0.0200	1.492026	1.492458
101	10	1	-6	62.9659	62.9634	0.0025	1.474976	1.475029
102	8	4	-3	63.7285	63.7234	0.0051	1.459152	1.459258
103	7	3	3	64.0111	64.0207	-0.0097	1.453391	1.453195

104	8	3	2	65.0028	65.0134	-0.0106	1.433594	1.433387
105	8	0	4	65.9165	65.8920	0.0245	1.415918	1.416386
106	2	3	7	67.2831	67.2990	-0.0159	1.390443	1.390153
107	1	3	-8	67.6220	67.6225	-0.0005	1.384296	1.384287
108	1	5	5	68.7200	68.7107	0.0093	1.364832	1.364994
109	7	5	-3	69.0997	69.1062	-0.0064	1.358257	1.358146
110	7	3	-8	69.7607	69.7685	-0.0078	1.346995	1.346864
111	3	6	1	70.3788	70.3802	-0.0014	1.336673	1.336650
112	12	1	-2	71.2098	71.1997	0.0101	1.323100	1.323262
113	9	0	-9	72.0235	72.0113	0.0122	1.310141	1.310333
114	8	0	5	72.3790	72.3804	-0.0013	1.304579	1.304558
115	2	6	-4	73.0009	73.0046	-0.0037	1.294992	1.294935
116	12	2	-3	73.3905	73.3853	0.0052	1.289077	1.289156
117	0	6	4	73.8753	73.8725	0.0028	1.281812	1.281853
118	1	5	6	74.1796	74.1766	0.0030	1.277305	1.277348
119	8	5	0	75.0217	75.0335	-0.0118	1.265042	1.264872
120	10	4	-5	75.6552	75.6730	-0.0179	1.256016	1.255764
121	2	5	-7	75.9135	75.9158	-0.0022	1.252383	1.252352
122	8	5	-5	76.2065	76.2136	-0.0071	1.248296	1.248198
123	9	4	2	77.8263	77.8104	0.0159	1.226314	1.226524
124	12	3	-3	78.2940	78.2925	0.0015	1.220156	1.220175
125	6	6	1	79.3502	79.3465	0.0037	1.206545	1.206593
126	5	1	8	79.5943	79.5848	0.0095	1.203458	1.203577
127	13	2	-2	81.1730	81.1726	0.0004	1.183991	1.183996
128	14	0	-4	83.1271	83.1240	0.0031	1.161051	1.161086
129	2	0	10	83.6355	83.6271	0.0084	1.155281	1.155376
130	3	3	9	86.9193	86.9181	0.0012	1.119875	1.119888
131	3	7	3	88.2043	88.2123	-0.0080	1.106847	1.106768